

Radiometer design analysis based upon measurement uncertainty

Paul Racette

NASA Goddard Space Flight Center, Greenbelt, Maryland, USA

Roger H. Lang

Department of Electrical Engineering and Computer Science, George Washington University, Washington, DC, USA

Received 25 July 2004; revised 10 September 2004; accepted 25 May 2005; published 17 September 2005.

[1] This paper introduces a method for predicting the performance of a radiometer design based on calculating the measurement uncertainty. The variety in radiometer designs and the demand for improved radiometric measurements justify the need for a more general and comprehensive method to assess system performance. Radiometric resolution, or sensitivity, is a figure of merit that has been commonly used to characterize the performance of a radiometer. However, when evaluating the performance of a calibration design for a radiometer, the use of radiometric resolution has limited application. These limitations are overcome by considering instead the measurement uncertainty. A method for calculating measurement uncertainty for a generic radiometer design including its calibration algorithm is presented. The result is a generalized technique by which system calibration architectures and design parameters can be studied to optimize instrument performance for given requirements and constraints. Example applications demonstrate the utility of using measurement uncertainty as a figure of merit.

Citation: Racette, P., and R. H. Lang (2005), Radiometer design analysis based upon measurement uncertainty, *Radio Sci.*, 40, RS5004, doi:10.1029/2004RS003132.

1. Introduction

[2] Radiometer calibration is becoming more important as radiometric measurements are being used to derive greater geophysical information. New applications for microwave and millimeter wave radiometer data are driving the need for improved radiometric resolution and correspondingly improved accuracy. Finer resolution permits enhanced discrimination of changes in physical parameters from background noise. Accuracy is important for comparing temporal and spatial measurements made from one or many sensors and for using measurements to retrieve parameters by inversion of physical models. Examples of parameters requiring improved resolution and accuracy include the retrieval of sea surface salinity, precipitable water vapor, liquid and ice water path, and vector wind measurements. For a discussion on the principles of radiometry see *Ulaby et al.* [1981], *Kraus* [1966], and *Rohlfis and Wilson* [1996].

[3] At the core of all radiometers is a calibrated receiver [*Skou*, 1989]. A radiometer receiver is shown

in Figure 1a. Noise power with equivalent brightness temperature T_{sys} enters the receiver and is converted to the output signal v . (In this paper we assume the Raleigh-Jeans limit of the Planck function, and thus brightness temperature is used as a measure of the band-limited detected power.) The system noise temperature at the receiver input is $T_{\text{sys}} = T_{\text{rec}} + T_A$, where T_A is the radiant power at the input of the radiometer antenna and T_{rec} is the receiver noise temperature referred to the receiver input. The radiometer response defines the relationship between v and T_A ; for radiometers utilizing square law detection, the response is linear and characterized by a slope and offset. The radiometer response fluctuates because of inherent instabilities in the radiometer electronics. Calibration is the process by which the radiometer response is estimated. Through calibration an estimate of T_A can be derived from the output signal v . The scheme employed to achieve calibration is central to the design of any radiometer; there exist many techniques for calibrating radiometers.

[4] The advent of the Dicke radiometer in the 1940s spawned radio astronomy and microwave radiometry [*Dicke*, 1946; *Buderi*, 1996]. Since then many improvements in radiometric measurement techniques have been developed. Many papers are written on radiometer

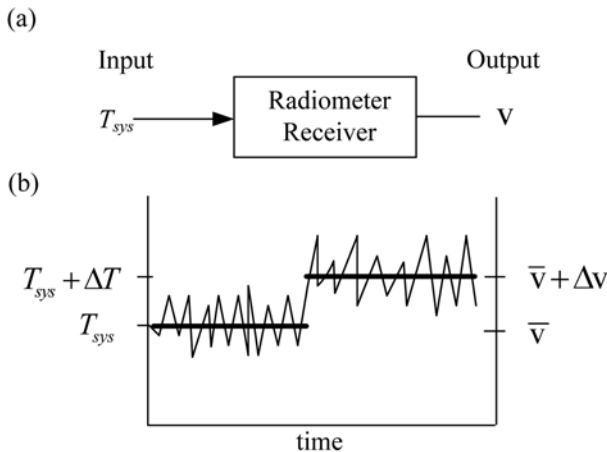


Figure 1. (a) Illustration of a basic radiometer model with input brightness temperature T_{sys} and output voltage v . (b) Graph illustrating the principle of measurement resolution.

designs and techniques for analyzing radiometer performance. In recent years the number of operating radiometer systems and variations in radiometer designs have increased. Advances in RF technology, system control, and numerical processing have greatly expanded the envelope of radiometer capabilities. Today there exist a great number of radiometer designs and nearly as many different implementations of calibration algorithms. Wide variation in calibration designs combined with the need for improved measurements are justification for more general and comprehensive analysis tools for predicting radiometer performance than currently exists.

[5] The primary objective of this paper is to present a generalized technique by which system calibration architectures and design parameters can be studied to optimize instrument performance for a set of given requirements and constraints. A generalized technique for analyzing radiometer designs should provide the means to evaluate the following: trade-off between time observing the measurand (i.e., the quantity of T_A being measured) and time spent calibrating, effects of interpolating and extrapolating the calibration, influence of calibration reference temperatures on the uncertainty, and influence of calibration frequency.

[6] A metric that satisfies these criteria is the uncertainty of measurement (or measurement uncertainty). Measurement uncertainty is a parameter that quantifies the dispersion of measured values about the mean value of the measurand (i.e., T_A) that could reasonably be expected [International Organization for Standardization (ISO), 1993]. In this paper, measurement uncertainty is defined as the mean square difference between the estimated value and the mean value of the measurand.

Applied to radiometry, measurement uncertainty includes the uncertainty due to the finite radiometric resolution inherent in the measurand observation and uncertainties associated with using imperfect calibration data. Measurement uncertainty as a figure of merit can be applied to the performance of all radiometers.

[7] The American National Standards Institute identifies two approaches for evaluating components of measurement uncertainty [American National Standards Institute (ANSI), 1997]. Type A evaluation is based upon statistical analysis of a series of observations. Type B evaluation is based on means other than analysis of observations and usually involves the assumption of a probability distribution function for those factors affecting measurement uncertainty. There is no difference in the nature of uncertainties derived from type A and type B analyses; the distinction is made only to reflect the means by which the uncertainty is evaluated. This paper only addresses measurement uncertainty associated with radiometer designs, and thus the discussion is limited to type B analyses.

[8] Measurement uncertainty as a function of calibration frequency depends on the nonstationary stochastic properties of the radiometer predetection circuit and receiver electronics. The principles underlying the use of measurement uncertainty as a figure of merit are illustrated by assuming the fluctuations in the radiometer response are wide sense stationary, that is, stationary in the first and second moment statistics. Analysis of nonstationary stochastic processes adds a layer of complexity and is not included in this presentation with the exception of brief discussions in sections 3 and 7.

[9] A discussion of previous works relevant to radiometer system analysis is presented in section 2. These works use resolution as a figure of merit for qualifying radiometer performance. Because of its importance to the theme of this paper, the definition of radiometric resolution is examined and the assumptions underlying the classic definition for resolution are reviewed in section 3 and Appendix A. The limitations in using radiometric resolution to evaluate calibration designs are discussed. In section 4 a general model for a radiometer design is introduced whereby the calibration architecture is divided into three tiers. A method for evaluating measurement uncertainty on the basis of stochastic signal theory is presented in section 5. Radiometric resolution is shown to be one component of the measurement uncertainty; other components arise from the estimation of the receiver response. The method presented is applicable to all radiometers with designs that can be decomposed into a set of measurement paths that represent total power mode observations. Examples illustrating the application of measurement uncertainty to evaluate different calibra-

tion schemes are given in section 6. A discussion and conclusion follow in sections 7 and 8.

2. Background

[10] Numerous papers have been written over the past fifty years that have led to improvements in radiometer system performance and analysis. Extensive analysis has been performed on the Dicke radiometer and total power configurations. Contemporary radiometer designs incorporate features of Dicke-type and total power mode measurements as well as external measurements to achieve calibration. In some radiometers the recorded output signal of the system is the difference between signals originating from the measurand and a standard reference. Usually the difference signal is generated by a synchronous detector that performs the subtraction function using analog electronics. Radiometers utilizing this reference-differencing detection scheme are often referred to as Dicke radiometers. In a switched-reference detection scheme, observations of the measurand are interleaved with observations of one or more references. Noise injection is a calibration technique where a preset noise power is added into the measurement path. Reference averaging is a technique in which multiple observations of a reference are used to improve the resolution of the reference measurement. In total power mode one or more observations of a measurand are made without interleaved observations of a reference.

[11] Reference-differencing radiometers have received extensive analysis in the literature [Tiuri, 1964; Wait, 1967; Bremer, 1979; Thomsen, 1984]. Wait [1967] derives a method using Fourier transforms for analyzing the resolution of reference differencing radiometers. Wait identifies a series of papers that analyze the performance of the reference differencing radiometer but yield differing results for the radiometric resolution. Wait resolves these differences by identifying the divergent assumptions, standardizing the notation, and pointing out errors in published results. A comparison of results is given in a table that contains the radiometric resolution for a number of modulation and correlation waveforms. Thomsen [1984] analyzes a reference-differencing radiometer with asymmetric switching, including the influence of gain fluctuations; however, in the limit of symmetric switching (50% duty cycle) with no gain fluctuations, his results differ by $2^{1/2}$ from those of Kraus [1966], Ulaby et al. [1981], Wait [1967], Bremer [1979], and others.

[12] The resolution of a reference-differencing radiometer may be improved by a technique presented by Bremer [1979]. Bremer demonstrates that significant improvement in performance can be achieved when the reference measurements are averaged over many cycles. Performance is optimized by increasing the portion of the duty cycle that is spent viewing the measurand and increasing the number of reference measurements aver-

aged to reduce the statistical uncertainty in the estimation of the reference value. The improvement in resolution may approach that of a total power mode measurement made over the same period. Reference averaging offers significant advantage over the traditional reference-differencing techniques and with the improvements in digital processing the implementation of reference averaging is greatly simplified. Today, reference averaging is commonly used in processing radiometer data.

[13] Hersman and Poe [2000] analyze the performance of the total power mode, improving upon previous analysis by including the effects of receiver gain fluctuation and calibration algorithm. In their presentation, radiometric resolution is used as the figure of merit and is defined to be proportional to the integral of the product of the receiver postdetection transfer function and the power spectrum of the square law detector output (see Appendix A, (A16)). The resulting model accounts for system noise temperature, nonuniform power spectral densities, and processing algorithm parameters such as the calibration period and integration times. Although a formula is presented for a two-point calibration [see Hersman and Poe, 2000, equation (9)], the approach fails to account for nonuniform noise components due to the receiver switching between sources. This shortcoming is avoided by assuming the measurand and calibration references have the same noise temperature. An upper limit on the resolution is obtained by setting the observed sources of emission equal to the hottest reference. Peckham [1989] extends their work by deriving a set of optimum weights that minimizes the variance of the difference between the weighted average of calibration and measurand samples in the presence of $1/f$ -type fluctuations in the receiver. In the limiting case with no gain fluctuations and uniform weighting of the reference measurements the results of Hersman and Poe [2000] agree with those presented by Bremer [1979].

[14] The references cited above use radiometric resolution as basis for assessing radiometer system performance. Measurement uncertainty is a more appropriate figure of merit for evaluating and comparing radiometer designs. The difference between radiometric resolution and measurement uncertainty is more than semantic. In section 5 resolution is shown to be one component of the measurement uncertainty and that other components arise from the application of imperfect calibration data. Recognizing the distinction facilitates performance analysis for all types of radiometers. In section 3 radiometric resolution is defined and evaluated for a simple direct detection radiometer.

3. Radiometric Resolution

[15] Radiometric resolution is defined to be the minimum change in the input signal level that can be resolved

at the output of the radiometer receiver. Figure 1b illustrates the relationship between the receiver input noise power and the output signal as a function of time. The radiometer output signal fluctuates because of the inherent stochastic properties of emission and receiver electronics. The mean output signal level, \bar{v} , is indicated on the right-hand side of Figure 1b and is given by

$$\bar{v}(T_{\text{sys}}) = E\{v(t)\}|_{T_{\text{sys}}}, \quad (1)$$

where the ensemble average includes all possible outputs, $v(t)$, that correspond to the input level T_{sys} . A change of signal (ΔT) is considered resolvable at the radiometer output if the ratio of the power in the signal change, ΔS_0 , to signal noise power at the output, N_0 , is equal to or greater than 1 [Dicke, 1946; Kelly et al., 1963; Wait, 1967], that is,

$$\frac{\Delta S_0}{N_0} \geq 1. \quad (2)$$

The signal noise power is proportional to the variance of the output signal evaluated at the receiver input noise temperature, T_{sys} ,

$$N_0 \propto \sigma_v^2|_{T_{\text{sys}}} = E\{v(t)v(t)\}|_{T_{\text{sys}}} - E^2\{v(t)\}|_{T_{\text{sys}}}. \quad (3)$$

The power in the change of signal is found by truncating the Taylor series expansion of $\bar{v}(T_{\text{sys}})$ at the second term for small ΔT , that is,

$$\bar{v}(T_{\text{sys}} + \Delta T) = \bar{v}(T_{\text{sys}}) + \Delta T \cdot \left. \frac{\partial \bar{v}}{\partial T} \right|_{T_{\text{sys}}}. \quad (4)$$

For a receiver with a square law detector, the relationship between \bar{v} and T_{sys} is linear; thus all the change in signal power is contained in the second term of the expansion. The power in the change of the output signal is

$$\Delta S_0 \propto (\bar{v}(T_{\text{sys}}) - \bar{v}(T_{\text{sys}} + \Delta T))^2 = \left(\Delta T \cdot \left. \frac{\partial \bar{v}}{\partial T} \right|_{T_{\text{sys}}} \right)^2. \quad (5)$$

Substituting (3) and (5) into (2), noting that the proportionality constant is the same, and solving for $(\Delta T)^2$ yields the classic formula

$$(\Delta T)^2 = \frac{\sigma_v^2}{\left(\left. \frac{\partial \bar{v}}{\partial T} \right|_{T_{\text{sys}}} \right)^2}. \quad (6)$$

The minimum detectable change in signal at the input is equal to the noise power at the output times the reciprocal of the squared response of the system evaluated at T_{sys} . Sometimes radiometric resolution is referred to as the noise equivalent temperature difference, that is, "NE ΔT ,"

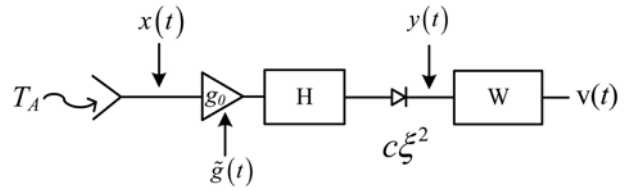


Figure 2. Block diagram of a direct detection radiometer making a total power mode measurement. The radiometer comprises an antenna, amplifier, predetection filter, square law detector, and postdetection filter.

or sensitivity. Peculiar to microwave engineering, sensitivity is synonymous to resolution. However, in other engineering disciplines, sensitivity is more commonly used to describe the change of a system output per change in input stimulus (or its reciprocal) [ISO, 1993; Institute of Electrical and Electronics Engineers, 1996; Van Putten, 1996]. The square root of the denominator in (6) is then the radiometer sensitivity. To be more consistent with the engineering community at large, resolution, or more specifically radiometric resolution, is preferred over sensitivity to describe (6).

[16] Figure 2 shows a model of a direct detection radiometer operating in total power mode. Noise power T_A enters the radiometer through an antenna. The radiometer receiver comprises an amplifier (g_0), predetection filter (H), square law detector, and a postdetection filter (W). The system noise temperature at the receiver input is $T_{\text{sys}} = T_A + T_{\text{rec}}$. The radiometer output is the voltage $v(t)$. Evaluating (6) for this radiometer model leads to the classic definition of radiometric resolution [Dicke, 1946; Rohlf's and Wilson, 1996]

$$\Delta T \cong \frac{T_{\text{sys}}}{\sqrt{B\tau}}, \quad (7)$$

where B is the bandwidth of the predetection filter and τ is the postdetection integration time constant. These terms are defined by Tiuri [1964] and are given in Appendix A. Rohlf's and Wilson [1996] present a derivation of (7) based upon stochastic signal theory. Le Vine [1990] presents a derivation of the resolution for a correlation receiver in an interferometer and shows how the result yields (7) in the limiting case of zero displacement in the antenna elements. In Appendix A, the radiometric resolution of a direct detection radiometer receiver with gain fluctuations is evaluated. The amplifier gain, $g(t)$, is modeled as a wide sense stationary random process with mean g_0 . For a receiver with gain fluctuations, (6) leads to

$$\Delta T \cong T_{\text{sys}} \cdot \left(\frac{1}{B\tau} + \left(\frac{\Delta G}{G} \right)^2 \right)^{1/2}, \quad (8)$$

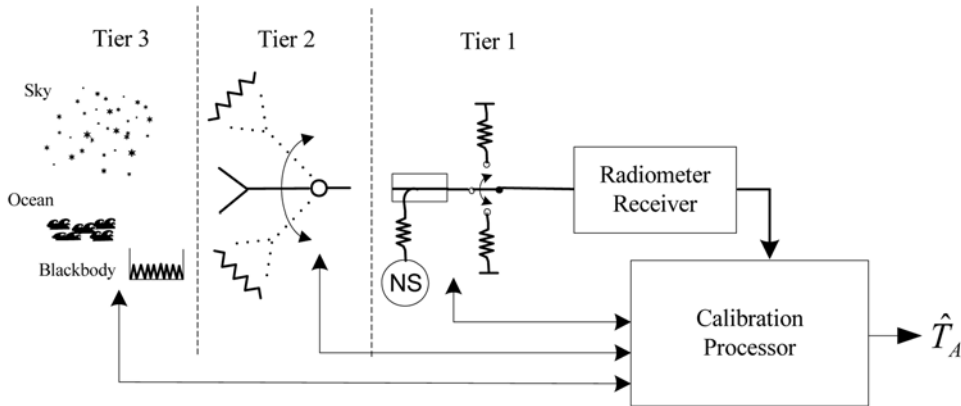


Figure 3. Generic model for radiometer calibration architecture illustrating three tiers of calibration. Tier 3 comprises calibration references external to the radiometer, for example, cosmic background radiation and ocean surface. Calibration references that are included as part of the radiometer system and that are observed through the antenna are in tier 2. Calibration references internal to the radiometer receiver and not observed through the antenna are in tier 1, for example, noise source injection.

where

$$\left(\frac{\Delta G}{G}\right)^2 = \left(\frac{2}{W(0) \cdot g_0}\right)^2 \int d f S_{\bar{g}}(f) |W(f)|^2,$$

and where $S_{\bar{g}}(f)$ is the power spectrum of the fluctuating component of $g(t)$ and $W(f)$ is the frequency response of the postdetection filter.

[17] Essential to the derivation of (8) is the assumption that $g(t)$ is wide sense stationary. Some authors [Kunzi and Magun, 1977; Hersman and Poe, 2000; Thomsen, 1984; Peckham, 1989] use

$$S_{\bar{g}}(f) \propto 1/f^\gamma$$

to evaluate (8), even though such a spectrum violates the Wiener-Khinchin theorem for $\gamma \geq 1$ [Davis et al., 1996]. One might argue that over a certain interval the gain fluctuations may be considered stationary, and hence the Fourier relationship between the autocorrelation function and power spectrum exists. In evaluating the influence of calibration frequency on measurement uncertainty, the interval of interest is on the same timescale that the fluctuations in the receiver become nonstationary. The assumption that the stochastic properties of the receiver are stationary may not be justified when studying the interaction between calibration frequency and receiver fluctuations. For this reason, the degree of stationarity [Huang et al., 1998] should be considered when evaluating temporal factors in the calibration algorithm.

[18] The effect of switching between calibration references on radiometric resolution of periodically calibrated

radiometers has been investigated [Bremer, 1979; Hersman and Poe, 2000]. Inevitably, calibration involves observations of references of different brightness temperatures. Evaluation of the output noise power when the input signal power changes when viewing different sources is nontrivial. Difficulty arises in computing the square law detector output and its convolution with the postdetection transfer function of the radiometer. Furthermore, (6) is evaluated at the system noise temperature. When a radiometer observes sources with different noise temperatures to achieve calibration, T_{sys} necessarily changes. Thus evaluating (6) in the context of a calibration algorithm is inconsistent with its definition. In the literature these complexities have been avoided by assuming the temperature of the measurand and calibration references are equal, thus limiting the usefulness of radiometric resolution as a figure of merit for the performance of a radiometer.

[19] An alternative approach is to consider the measurement uncertainty that includes the resolution of the measurand observation as well as uncertainty associated with applying the calibration data. Before developing a method for evaluating measurement uncertainty, in section 4 a general model is introduced that describes a wide variety of calibration architectures.

4. General Radiometer Calibration Model

[20] The calibration architecture of most microwave radiometers can be divided into three tiers as illustrated in Figure 3. Measurements from one or more of the three tiers are used to calibrate the radiometer response. A data processor controls the timing of the calibration reference

observation sequence as well as records pertinent data for utilizing the references. In some systems data may be processed in real time to produce estimates of the antenna brightness temperature and others rely on post-processing of the data to calculate the estimates.

[21] First-tier calibration consists of calibration references that are switched into the receiver path after the antenna. Calibration structures that fit into this first category include temperature-controlled waveguide terminations switched into the receiver path using waveguide switches and active noise sources injected using directional couplers. The first tier is most often used to compensate for fluctuations in the active components of a receiver. Though one or more internal references can be used to track fluctuations in the receiver response, the internal references do not measure fluctuations that occur in circuitry beyond the plane of the reference measurement, for example, antenna losses. Usually the equivalent antenna brightness temperature of the references have to be determined through either second- or third-tier calibration. First-tier calibration is utilized when second- or third-tier calibrations cannot be performed sufficiently rapid to track receiver fluctuations. Descriptions of radiometers that use first-tier calibration can be found in work by *Hach* [1968], *Conglong et al.* [1986], *Ruf et al.* [1995], *Racette et al.* [1998], and *Tanner and Riley* [2003].

[22] The second tier comprises calibration structures that provide a means of calibrating the system response, including the effects of the antenna and coupling components. Typically, the antenna pattern is projected onto one or more isothermal blackbody radiators. In systems that utilize a second-tier structure, characterizing system response is straightforward and can yield accurate calibration since the entire signal path including lossy antenna components is included in the calibration. Several factors limit the practicality of implementing second-tier architectures. Blackbody radiators that can envelop the antenna aperture are large, massive, expensive, and prone to errors caused by thermal gradients. Usually, a mechanism is needed to switch the field of view of the antenna from the measurand to the calibration reference(s), thus complicating the design of the instrument. Such switching mechanisms are typically slow and contribute to the measurement uncertainty. The Millimeter-Wave Imaging Radiometer [*Racette et al.*, 1996], MARSS [*McGrath and Hewison*, 2001], and the Advanced Microwave Sounding Unit-B (AMSU-B) [*Saunders et al.*, 1995] are examples of radiometers that utilize second-tier calibration. The Polarimetric Scanning Radiometer utilizes both first- and second-tier calibration structures in its calibration scheme [*Corbella et al.*, 2002]. In some radiometer designs the distinction between tier 1 and tier 2 architectures is not clearly delineated. For example, in the TRMM Microwave

Imager, a blackbody radiator and cold space mirror are moved between the primary antenna reflector and the feed horns [*Wentz et al.*, 2001].

[23] Although second-tier calibration provides a means of estimating the system response that includes the effects of antenna losses and coupling mechanisms, additional parameters may be necessary to correct for instrument-specific effects such as cross coupling of the calibration references [*Racette et al.*, 1995]. Third-tier calibration utilizes measurements external to the instrument. These measurements can then be used to estimate parameters used in the instrument calibration. External references can be blackbody radiators or environmental sources of emission with known properties. Examples of environmental references include: cosmic radiation, tip-curve calibration, and ocean surface. The third tier often provides the most accurate reference for calibration because the measurements encompass entire system effects and external references, for example, cosmic radiation, can be as close to an absolute standard that exists. External calibration can also correct for instrument effects that are not measured in first- or second-tier calibrations. Nevertheless, third-tier calibration usually comes with difficulties associated with making the measurement. External reference measurements usually cannot be performed with frequency adequate to track fluctuations in the receiver response. Because of its ability to accurately and precisely characterize entire system effects, third-tier calibration is often used to tweak parameters, for example, antenna coupling losses, effective noise source temperature, etc., in the system equations that describe the radiometer response. An example of the application of third-tier architecture applied to calibrating a radiometer is given by *Ruf* [2000]. *Ruf* describes a technique whereby the properties of the ocean surface brightness temperature are used to correct for a drift in the isolation of a ferrite switch in the TOPEX/Microwave Radiometer.

[24] The Microwave Water Vapor Radiometer (MWR) used by the Department of Energy's Atmospheric Radiation Measurement program is an example of a radiometer that operationally utilizes all three tiers to achieve calibration [*Liljegren*, 2000]. A noise source is injected into the receiver path using a directional coupler. A rotating mirror projects the antenna pattern at an internal blackbody and over a range of elevation angles across the sky. The relation between atmospheric opacity and elevation angle, that is, tip-curve calibration [*Han and Westwater*, 2000], is used to track the effective noise source temperature and system losses.

[25] It is usual to include parameters in the radiometer calibration to correct for nonidealities in the instrument, for example, insertion loss, reflections, coupling. Many papers have been written on radiometer system models, parameters to include in the calibration, and techniques

for estimating calibration parameters. A technique to correct for coupling between calibration references and the measurand is given by *Racette et al.* [1995]. A technique for transferring internal calibration measurements (tier 1) to an equivalent antenna brightness temperature is given by *Corbella et al.* [2002]. Insertion loss and mismatch effects on radiometric measurements are discussed by *Hach* [1968], *Ulaby et al.* [1981], *Ruf et al.* [1995], *Stelzried* [1968], and *Miller et al.* [1967]. Parameters used for calibration are specific to the system design; values of the parameters and their corresponding uncertainties are specific to the hardware used in the design implementation.

[26] In section 5 the uncertainty in the calibrated estimate of the measurand, that is, measurement uncertainty, is derived. The measurement uncertainty is a function of the individual uncertainties of all the values that go into calculating an estimate of the measurand. The technique can be applied to systems utilizing calibration measurements from one or a combination of tier 1, 2 or 3 architectures.

5. Calculation of Measurement Uncertainty

[27] In this section a technique is presented for evaluating the measurement uncertainty of a radiometer design. First, the design is decomposed into a set of subsystems, one for each state of the radiometer. Each state represents a total power mode observation. The output signal of each subsystem is treated as a separate random process. The radiometer output is then considered as a sequence of samples obtained from the different random processes. An estimate of the measurand is calculated from samples of these random processes. The measurement uncertainty is computed from the statistics of the samples and the functional form of the estimator. The technique can be applied to all radiometers with designs that can be decomposed into a set of subsystems that represent total power mode observations.

5.1. Model Decomposition and Measurement Estimator

[28] Figure 4a shows a model of a radiometer system that has $N + 1$ measurement states. The states of the radiometer correspond to observations of the measurand, external calibration references, for example, T_{sky} , shown in Figure 4a, or one of a number of calibration references. Measurement states may also include additive noise coupled into the measurement path as indicated in Figure 4a. The radiometer output depends on the radiometer state. At any instance in time the radiometer output corresponds to only one of its possible $N + 1$ states; the timing of the state sequence is prescribed by

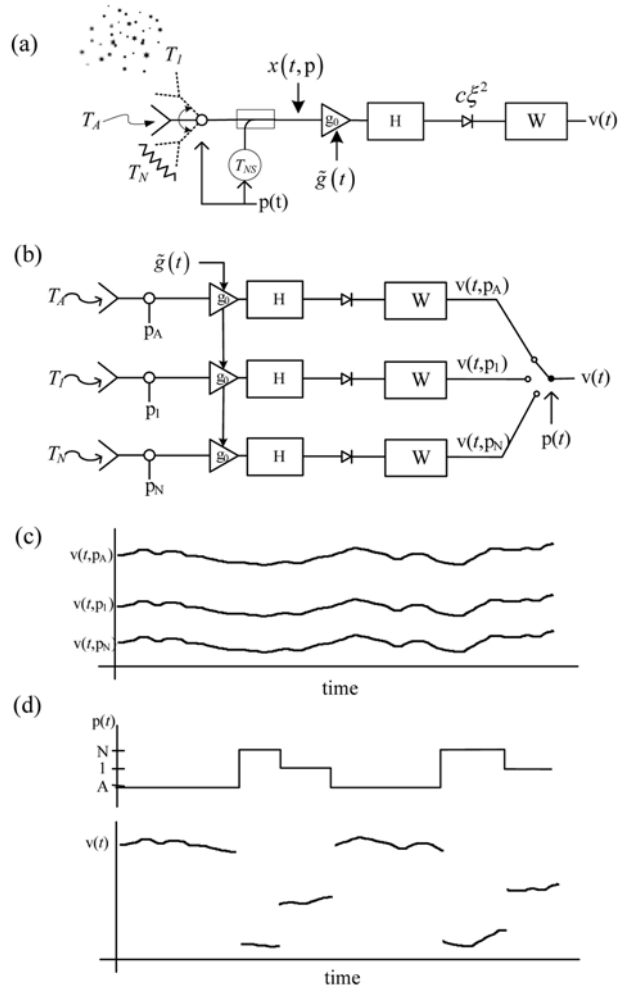


Figure 4. (a) Model of a radiometer with a switch used to view one of $N + 1$ radiation sources. The switch position is controlled by $p(t)$. (b) Radiometer expanded as a set of subsystems with each subsystem representing a total power mode measurement. (c) Signals out of the total power mode measurement. (d) Radiometer output, which is a sequence of samples from the set of random processes.

$p(t)$, where $p \in \{A, 1, \dots, N\}$. Observations of the measurand correspond to the state $p = A$. Figure 4b illustrates a representation of the radiometer as a set of subsystems, one for each possible value of p . Each subsystem is mathematically modeled by a characteristic equation that describes the random process at its output. The random processes are treated as though each simultaneously exists. Figure 4c shows a time series of the $N + 1$ processes. The output of the radiometer is a sample of only one of the processes at any given time. By decom-

posing the radiometer design in this way, transient effects between samples are neglected. Figure 4d shows a time series of the radiometer output for a particular state sequence.

[29] Each subsystem is treated as a radiometer receiver operating in total power mode. The mathematical model for the voltage output is given by (A6) in Appendix A. The model includes inherent fluctuations of the receiver input and instability of the receiver gain. Although the radiometer state is not explicitly shown, its effect is implicit in the value of T_{sys} . For any p , the input to the receiver, $x(t, p)$, is defined to be a zero mean wide sense stationary Gaussian random process with a white power spectrum given by

$$S_x(f, p) = kT_{sys}(p) = k(T_{rec} + T_p), \quad (9)$$

where k is Boltzmann's constant and T_{rec} is the receiver noise temperature referred to the receiver input. T_p is the equivalent antenna brightness temperature [Corbella *et al.*, 2002] referred to the receiver input for the radiometer state designated by p . For a lossless system, T_p is equal to the antenna temperature but T_p may also include noise contribution from system losses or injected noise, for example, through a directional coupler. The output voltage is a function of time and radiometer state, $v(t, p)$. The expected value of $v(t, p)$ is evaluated in Appendix A (see (A6)–(A8)) and is shown to be a linear function of T_p ,

$$E\{v(t, p)\} = \bar{v}_p = \mu T_p + \beta, \quad (10)$$

where μ is the receiver gain and β is the offset and are defined by (A9) and (A10), respectively. The linear relationship arises from the square law detection of the input signal.

[30] When sampling the radiometer output, it is not possible to measure the mean value of voltage output given by (10) with zero uncertainty. Thus the radiometer output is rewritten as the sum of the mean, \bar{v}_p , and a fluctuating component \tilde{v} ,

$$v(t, p) = \bar{v}_p + \tilde{v}(t, p) = \mu T_p + \beta + \tilde{v}(t, p), \quad (11)$$

where $\tilde{v}(t, p)$ is a zero mean random process. The variance of $\tilde{v}(t, p)$ can be found from the covariance of the output $v(t, p)$ given by (A12) in Appendix A since $\sigma_{v_p}^2 = \sigma_{\tilde{v}_p}^2$. In anticipation of forming an estimator for the antenna brightness temperature, (11) is rewritten to express the brightness temperature as the sum of two random variables, that is,

$$T_p = mv(t, p) + b + \varepsilon(t, p), \quad (12)$$

where $m = \mu^{-1}$, $b = -\beta\mu^{-1} = T_{rec}$, and $\varepsilon(t, p) = -\tilde{v}(t, p)\mu^{-1}$. The slope m and offset b define the mean system response.

[31] When making measurements with a radiometer, the brightness temperature at the radiometer input is usually not known but is estimated from a measurement of the output voltage. Equation (12) is used as a model to define an estimator for the input brightness temperature. At a particular instance in time the measured output is v_p ($p = A$ for the measurand) and the estimator for the input brightness temperature is

$$\hat{T}_p = mv_p + b. \quad (13)$$

The expected value of the estimator is

$$E\{\hat{T}_p\} = E\{mv_p + b\} = m\bar{v}_p + b = T_p. \quad (14)$$

The variance of the estimator is

$$\sigma_{\hat{T}_p}^2 = E\left\{\left(\hat{T}_p - T_p\right)^2\right\} = E\left\{\varepsilon_p^2\right\} = \frac{\sigma_{v_p}^2}{\mu^2}. \quad (15)$$

The estimator \hat{T}_p is a random variable with mean and variance given by (14) and (15), respectively. The fluctuating component ε_p arises from the stochastic nature of the signal at the input of the receiver and instabilities within the receiver. This fluctuation is indistinguishable from fluctuations that may exist in T_p . The standard deviation of the estimator given by the square root of (15) is the standard uncertainty as defined by ANSI [1997] and is equal to the radiometric resolution given by (6), since $\mu = \frac{\partial \bar{v}_p}{\partial T_p}$. The uncertainty as expressed by (15) is based on the mean system response defined by m and b and, hence does not include uncertainty due to imperfect calibration.

5.2. Estimator of the Measurand and Measurement Uncertainty

[32] Generally, m and b in (13) are not known but must be estimated by calibrating the system. Therefore the uncertainty in the estimated antenna brightness temperature should include the uncertainty in the estimates of m and b . An estimate of the measurand, that is, the unknown antenna brightness temperature, must be obtained by using an estimate of the system response. An estimate of the measurand is derived from samples obtained from the different radiometer states. In the most general case, the estimator may be expressed as a function of random variables,

$$\hat{T}_A = f(x_1, x_2, \dots, x_K). \quad (16)$$

The set of random variables, x_i for $i \in \{1, \dots, K\}$, may include voltages, brightness temperatures of calibration references, physical temperatures of radiometer components, insertion losses, antenna beam efficiencies, etc., that is, any element in the system that contributes

uncertainty to the estimator. The estimator, \hat{T}_A , differs from \bar{T}_A given by (13); \hat{T}_A is an estimate of the antenna brightness temperature based upon estimates of the system response, whereas, \bar{T}_A is an estimate of the antenna brightness temperature for a known system response, that is, a perfectly calibrated system.

[33] The uncertainty in the estimator is obtained by evaluating

$$\sigma_{\hat{T}_A}^2 = E\left\{(\hat{T}_A - T_A)^2\right\}, \quad (17)$$

where $T_A = f(\bar{x}_1, \bar{x}_2, \dots, \bar{x}_K)$ and $\bar{x}_i = E\{x_i\}$. To evaluate (17), a multivariate Taylor series expansion about the mean value of each random variable is performed on (16). Substituting the series expansion into (17) leads to the law of propagation of uncertainty given by *ANSI* [1997]. By assuming the estimator is well approximated by a linear expansion for values of anticipated fluctuations, the series can be truncated at the second term. The first term in the series expansion is T_A and cancels with T_A in (17). Thus

$$\sigma_{\hat{T}_A}^2 = \sum_{k=1}^K \sum_{i=1}^K E\{(x_k - \bar{x}_k)(x_i - \bar{x}_i)\} f_{x_k} f_{x_i}, \quad (18)$$

where

$$f_{x_i} = \left. \frac{\partial}{\partial x_i} f(x_1, x_2, \dots, x_K) \right|_{x_1=\bar{x}_1, x_2=\bar{x}_2, \dots, x_K=\bar{x}_K}. \quad (19)$$

By assuming all of the random variables are independent, the uncertainty reduces to

$$\sigma_{\hat{T}_A}^2 = \sum_{i=1}^K \sigma_{x_i}^2 f_{x_i}^2, \quad (20)$$

where $\sigma_{x_i}^2$ is the variance of the random variable x_i . *Randa* [1998] provides an example application of the law of propagation of uncertainty by calculating the uncertainty in noise-temperature measurements of noise source standards. A comprehensive discussion and treatment of measurement uncertainty including the case for correlated variables is given by *ANSI* [1997].

5.3. Least Squares Regression

[34] Selection of calibration architectures and optimization of design parameters can be made by evaluating the measurement uncertainty. However, evaluation of measurement uncertainty requires an estimator for the measurand. As with selecting a calibration architecture, there exists a great deal of freedom when developing an estimator even though the form of the estimator is constrained by the radiometer design and its sampled states. In the following we develop an estimator based on least squares regression (LSR). Though LSR cannot be applied to all radiometer designs, the framework dem-

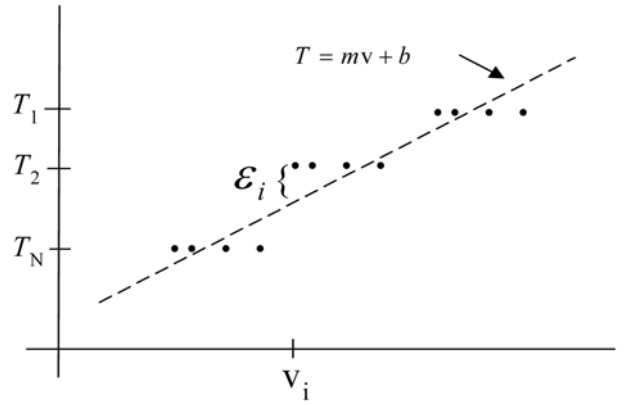


Figure 5. Graphical illustration of a calibration data set of n measurements made at N different temperatures with $n > N$. The dashed line is the response of the radiometer.

onstrates the utility of measurement uncertainty for performing trade studies on a wide variety of radiometer designs. The advantages and limitations of using LSR are discussed in section 7.

[35] Consider a set of measurements that is made up of observations of calibration references and the measurand at certain times. The measurement set is $\{v_A, v_1, \dots, v_n, T_1, \dots, T_n\}$. (Note that $\{v_p, T_p\}$ are values of the random variables $\{v_p, T_p\}$.) The set of measurements is used with (12) to form a set of characteristic equations,

$$\begin{aligned} T_A &= mv_A + b + \varepsilon_A \\ T_1 &= mv_1 + b + \varepsilon_1 \\ &\vdots \\ T_n &= mv_n + b + \varepsilon_n. \end{aligned} \quad (21)$$

As in (12), m and b represent the mean response of the system. The value of the measurand, T_A , is not known but must be estimated from the data set. The measured output, v_A , is used to estimate the measurand by

$$\hat{T}_A = \hat{m}v_A + \hat{b}, \quad (22)$$

where \hat{m} and \hat{b} are estimates of the system response. The value of ε_A in (21) is not known but its variance, $\sigma_{\varepsilon_A}^2$, is given by (15); its standard deviation is equal to the radiometric resolution of the measurand observation.

[36] Estimates of m and b are derived from the calibration measurements that comprise the remainder of the data set, that is, $\{T_i, v_i\}$, where $i \in \{1 \dots n\}$. The calibration measurement pairs consist of the recorded output voltage, v_i , and the reference brightness temperature, T_i . Figure 5 illustrates the set of measurements. Note that there can be

several measurements made at the same temperature T_i . Figure 5 shows that n measurements are made at N different temperatures with $N < n$. The ε_i are not part of the data set and are not known but represent the deviation of the measurement pairs, $\{T_i, v_i\}$, from the mean system response. When T_i is the mean or “true” antenna temperature, the variance of ε_i is given by (15). However, it is usual to approximate T_i through ancillary measurements and/or assumptions, for example, by measuring the physical temperature of a calibration reference and its emissivity. In this analysis, the “true” value of T_i is assumed to be constant; however, the knowledge of T_i is treated as a random variable. Thereby, the fluctuations in v_i are independent of the knowledge of the value of T_i . Subsequently, the “true” value of T_i is expressed as \bar{T}_i and uncertainty in the knowledge of \bar{T}_i is $\sigma_{\bar{T}_i}$.

[37] There are a number of different ways to use the data in (21) to derive estimates of the system response. For reasons discussed in section 7, LSR has been chosen as the framework to obtain \hat{m} and \hat{b} . The estimated system response is found by minimizing the sum of the squared errors, that is, by minimizing E where

$$E = \sum_{i=1}^n \varepsilon_i^2 = \sum_{i=1}^n (v_i \hat{m} + \hat{b} - T_i)^2. \quad (23)$$

Applying LSR to the data set yields [Draper and Smith, 1998]

$$\hat{m} = \frac{\sum_{i=1}^n (v_i - \langle v_i \rangle_n) T_i}{\sum_{i=1}^n (v_i - \langle v_i \rangle_n)^2} \quad (24)$$

and

$$\hat{b} = \langle T_i \rangle_n - \hat{m} \langle v_i \rangle_n, \quad (25)$$

where $\langle T_i \rangle_n$ and $\langle v_i \rangle_n$ are the arithmetic averages of the calibration data set given by

$$\langle T_i \rangle_n = \frac{1}{n} \sum_{i=1}^n T_i \quad (26)$$

and

$$\langle v_i \rangle_n = \frac{1}{n} \sum_{i=1}^n v_i. \quad (27)$$

Substituting (24)–(27) into (23) the antenna brightness temperature estimator is

$$\begin{aligned} \hat{T}_A &= (v_A - \langle v_i \rangle_n) \frac{\sum_{i=1}^n (v_i - \langle v_i \rangle_n) T_i}{\sum_{i=1}^n (v_i - \langle v_i \rangle_n)^2} + \langle T_i \rangle_n \\ &= f(v_A, v_1, \dots, v_n, T_1, \dots, T_n). \end{aligned} \quad (28)$$

Equations (24) and (25) are the best estimate of the slope and offset when all the measurements in (21) have an equal level of confidence, that is, ε_i have equal variance. However, when the variances of ε_i are not equal (which is usually the case), a better estimate of the slope is obtained using weighted least squares regression. When the ε_i in (21) are correlated, generalized least squares regression can be used [Draper and Smith, 1998]. So long as ε_i and ε_A have zero mean, \hat{m} , \hat{b} , and \hat{T}_A are unbiased estimators. Note that the estimator given by (28) does not include m , b , \hat{m} , or \hat{b} but that fluctuations in the receiver response are embedded in the statistics of the sampled pairs $\{T_i, v_i\}$.

[38] The measurement uncertainty of the estimator given by (28) is found by substituting (28) into (20). Here, all of the random variables that comprise the data set are assumed to be independent. This assumption implies that the covariance between samples of the receiver output (see (A17) in Appendix A and the discussion following it) is much smaller than the variance of the samples, that is, $C_v(\Delta t) \ll C_v(0)$ where Δt is the time interval between samples. As mentioned above, the stochastic fluctuations in the measured voltages are independent of the knowledge of the reference temperatures. The measurement uncertainty is evaluated and found to be

$$\begin{aligned} \sigma_{\hat{T}_A}^2 &= \sigma_{T_A}^2 + \frac{\sum (\sigma_{T_i}^2 + \sigma_{\bar{T}_i}^2)}{n^2} \\ &+ \frac{(T_A - \langle \bar{T}_i \rangle_n)^2 \sum (\bar{T}_i - \langle \bar{T}_i \rangle_n)^2 (\sigma_{T_i}^2 + \sigma_{\bar{T}_i}^2)}{\left(\sum (\bar{T}_i - \langle \bar{T}_i \rangle_n)^2 \right)^2} \\ &+ \frac{2(T_A - \langle \bar{T}_i \rangle_n) \sum (\bar{T}_i - \langle \bar{T}_i \rangle_n) (\sigma_{T_i}^2 + \sigma_{\bar{T}_i}^2)}{n \cdot \sum (\bar{T}_i - \langle \bar{T}_i \rangle_n)^2}, \end{aligned} \quad (29)$$

where the summations are performed over the $i = 1 \dots n$ measurements. In deriving (29), we make use of the equality of the partial derivatives, $f_{v_i}^2 = m^2 f_{T_i}^2$, and the relationships $\sigma_{T_i}^2 = m^2 \sigma_{v_i}^2$ and $\bar{T}_i = m \bar{v}_i + b$ to arrive at the simplified expression. Equation (29) expresses the uncertainty of the estimated brightness temperature in terms of the resolution of the measurand observation (σ_{T_i}), resolution of the reference measurements (σ_{T_i}), temperatures of the calibration references (\bar{T}_i), and uncertainty in the knowledge of the reference temperatures ($\sigma_{\bar{T}_i}$). This equation is the basis for making quantitative trade studies of the calibration algorithm for a radiometer design using an LSR estimator for the measurand. The first term on the right-hand side of (29),

$\sigma_{T_A}^2$, is the square of the radiometric resolution of the measurand. The next three terms arise from the uncertainty in the estimate of the system response and represent the effects of using imperfect calibration data. In the limit of perfect calibration, $\sigma_{T_i} \rightarrow 0$ and $\sigma_{\bar{T}_i} \rightarrow 0$, the measurement uncertainty converges to the radiometric resolution of the measurand.

[39] Before showing how (29) can be applied to study a system design, it is illustrative to consider the limiting case where $\sigma_{\bar{T}_i}^2 = 0$ and all $\sigma_{T_p}^2$'s, for $p \in \{A, 1, \dots, n\}$, are equal. Setting $\sigma_{T_i}^2 = \sigma_{T_A}^2$ and simplifying, (29) becomes

$$\sigma_{T_A}^2 = \sigma_{T_A}^2 \left(1 + \frac{1}{n} + \frac{(T_A - \langle \bar{T}_i \rangle_n)^2}{\sum (\bar{T}_i - \langle \bar{T}_i \rangle_n)^2} \right). \quad (30)$$

Several observations can be made with regard to (30). The uncertainty in the calibrated response is minimum when the measurement value T_A is equal to the mean of the calibration temperatures. The uncertainty is improved by increasing the separation of the calibration temperatures; the larger separation yields a larger value in the denominator of the third term on the right-hand side. The uncertainty is unbounded when all the reference measurements are made at the same reference temperature, that is, when $\bar{T}_i = \langle \bar{T}_i \rangle_n$ for $i = 1 \dots n$. Finally, the uncertainty is improved by increasing the number of calibration measurements. In the limit for increasing n , the uncertainty in the calibrated estimate converges to the radiometric resolution. These results are consistent with experiment design considerations for the regression of data as discussed by *Draper and Smith* [1998].

[40] Least squares regression provides a framework for calculating the measurement uncertainty by which the performance of a calibration design can be assessed. Application of the method is simple and straightforward. In section 6, examples illustrate how LSR can be used to study system design and evaluate the influence of design parameters on instrument performance.

6. Application of the Theory

[41] When designing a radiometer there are several constraints applied to the design on the basis of sampling requirements, operating environments, and limitations due to budgetary or more simply technical difficulties. Even with these constraints there usually exist many degrees of freedom in designing the calibration scheme for the system. In this section, measurement uncertainty is evaluated for different calibration schemes; the utility of measurement uncertainty as a figure of merit is demonstrated by evaluating the effect of reference temperature, number of references, and reference averaging

on the performance of the calibration design. In the following, uncertainty in knowledge of the reference temperatures is neglected, that is, $\sigma_{\bar{T}_i} = 0$, in the analysis.

6.1. Imaging Radiometer

[42] First consider a design based upon the Millimeter-wave Imaging Radiometer (MIR). A detailed description of the MIR can be found in work by *Racette et al.* [1996] and a description of the salient characteristics follows. The MIR has five receivers spanning 89 GHz to 340 GHz. The lack of electronic switches at these high frequencies and the short integration times required for imaging led to the decision of using total power mode. Calibration is achieved by periodically observing two blackbody references at different temperatures. The instrument is designed to fly aboard the NASA ER-2 high-altitude aircraft but has also been used for ground-based atmospheric measurements as well as laboratory studies [*Racette and Wang*, 1998].

[43] Images are generated by a rotating the antenna patterns across a field of view using a flat mirror canted at 45° angle. The across-track swath width is 100° centered about nadir. At cruising altitude of ~ 20 km the ER-2 airspeed is about 200 m/s. The nominal full width half-power beam width for each of the receivers is 3.5° . To achieve contiguous images at half altitude (~ 10 km) the instrument must scan the field of view every 3 s. The desire to avoid gaps in the images and the need for frequent calibration to circumvent errors in calibration due to drifts in the receiver gain and offset led to the decision to include calibration observations during each scan cycle. The constraint on the scan cycle period leads to a trade-off between time available to observe the measurand and time available to observe the calibration references. A latency interval exists during which time the mirror must switch between the calibration references and the beginning and end of the field of view. The latency interval also includes the settling time required for the mirror motion and postdetection filters. For the MIR, the latency interval is dominated by the rotation of the scan mirror. However, for a system utilizing electronic switches, the time to switch between calibration references and the measurand can be significantly shorter than the settling time of the receiver. Of course it is desirable to keep the latency interval as short as possible.

[44] The total scan period comprises three components as follows:

$$\tau_{tot} = \tau_s + \tau_{cal} + \tau_{lat}, \quad (31)$$

where τ_s is the time spent observing the measurand, τ_{cal} is the time spent calibrating, and τ_{lat} is the latency interval. A relationship between the pixel integration time and calibration integration time can be derived from (31).

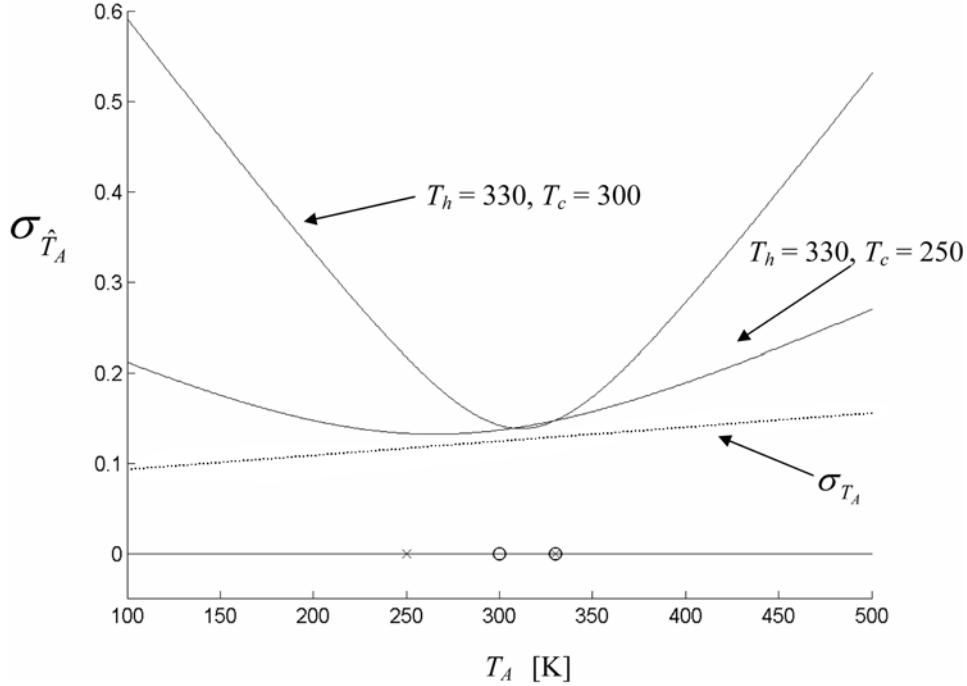


Figure 6. Standard measurement uncertainty versus measurand brightness temperature for two pairs of calibration target temperatures. The circles and crosses on the abscissa indicate the temperatures of the calibration references. The dotted curve shows the resolution of the measurand observation.

Assume there are M pixels for each swath scan and that $\tau_s = M\tau_A$ where τ_A is the pixel integration time. Furthermore, assume the integration time at each calibration reference is equal to τ_i and there are N calibration references, $\tau_{cal} = N\tau_i$. On the basis of the requirement for contiguous coverage the cycle period is $\tau_{tot} = 3$ s. For the MIR, there are $M = 56$ pixels, $N = 2$ calibration references, and $\tau_{lat} = 0.5$ s. Using these values a relation between the pixel integration time and calibration reference integration time is obtained,

$$\tau_A = \frac{2.5 - 2\tau_i}{56}. \quad (32)$$

Relationship (32) for τ_A and τ_i is used in Figures 6 and 7 to illustrate the trade-off between integration time and calibration reference temperature. Calculations use predetection bandwidth, $B = 1$ GHz, and the receiver noise temperature $T_{rec} = 500$ K. Regular (unweighted) least squares regression is used in the calculations. (A small improvement results from using weighted LSR.) A single set of calibration measurements, that is, $n = N$, are used and gain fluctuations are neglected, that is, $\tilde{g}(t) = 0$. In the figures that follow, the uncertainty in the measurand brightness temperature estimate is calculated using (29). The uncertainty in the calibration measure-

ments, σ_{T_i} , and the resolution of the measurand observation, σ_{T_A} , are calculated from (7) using

$$\sigma_p = (T_{rec} + T_p)(B\tau_p)^{-\frac{1}{2}}, \quad (33)$$

where $p \in \{A, 1, \dots, n\}$. Figure 6 shows the standard uncertainty in the estimate, \hat{T}_A , as a function of measurand brightness temperature, T_A . Two calibration references are viewed each for $\tau_i = 200$ ms. The pixel integration time is $\tau_A = 38$ ms. Three sets of curves are shown. The dotted curve shows the uncertainty in the estimate based solely on the resolution of the pixel measurement, σ_{T_A} . The other two curves illustrate the effect of calibration reference temperature on the measurement uncertainty. Markers on the abscissa indicate the temperatures of the calibration references for two cases. One calibration reference is maintained at 330 K. The other reference floats at the ambient temperature, which in flight is ~ 250 K; for laboratory measurements, the temperature of the ambient target is ~ 300 K. When the calibration data is interpolated the uncertainty in the estimate is near equal the resolution of the measurement. The curves show how the uncertainty in the estimate increases as the calibration data are extrapolated. The advantage of having large separation

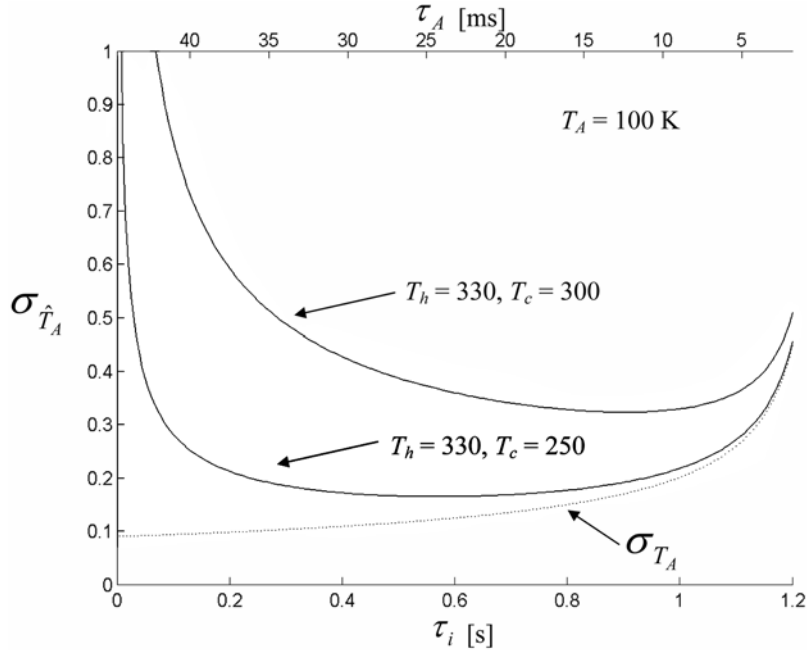


Figure 7. Standard measurement uncertainty as a function of time spent at each calibration reference (bottom abscissa) and time spent observing the measurand (top abscissa) for two pairs of calibration target temperatures. The dotted curve shows the resolution of the measurand observation.

in the calibration reference temperatures is apparent. For $T_A = 100$ K the uncertainty is improved by nearly a factor of 3 with the larger separation of reference temperatures.

[45] Figure 7 shows how the measurement uncertainty changes with calibration measurement integration time. The measurand brightness temperature is $T_A = 100$ K. As indicated, the two curves represent the same calibration reference temperatures shown in Figure 6. Again the dotted curve shows the standard uncertainty of measurement based solely on the resolution at the measurand temperature. The top abscissa indicates the pixel integration time; the bottom abscissa indicates the calibration reference integration time. On the left side of the plot, uncertainty is dominated by uncertainty in the regression of the calibration data; not enough time is spent calibrating. On the right side, uncertainty is dominated by the resolution of the measurand observation; not enough time is spent observing the measurand. The optimum integration times correspond to the uncertainty minima. For laboratory measurements when the extrapolation of the calibration data is greater, it is advantageous to spend more time calibrating than when in flight. The curves illustrate how calibration reference temperatures affect the trade-off between time spent calibrating and observing the measurand.

[46] Figures 6 and 7 demonstrate how analysis of measurement uncertainty can be used for assessing the

trade-off between performance and system parameters. For example, the advantages of achieving wider temperature separation for the calibration references can be weighed against the additional costs incurred and the performance gained.

6.2. Multiple References

[47] Some radiometers use measurements from more than two references to estimate the system response [Racette *et al.*, 1998; Blackwell *et al.*, 2001; Tanner and Riley, 2003]. Figure 8 shows how the estimate uncertainty changes with the number of references, that is, N , used for calibration. Three cases are shown for $N = 2$, $N = 3$, and $N = 100$. The reference temperatures are evenly distributed between $T_c = 250$ K and $T_h = 330$ K; for example, for $N = 3$ the reference temperatures are $T_1 = 250$ K, $T_2 = 290$ K, and $T_3 = 330$ K. The calculations assume a fixed time interval for calibration, that is, $\tau_{cal} = 0.4$ s; the integration times for each reference observation are equal, that is, $\tau_i = \tau_{cal}N^{-1}$. The latency interval remains fixed, $\tau_{lat} = 0.5$ s, independent of the value of N . As in Figure 6 the pixel integration time is $\tau_A = 38$ ms. The measurement uncertainty is minimum when only two references are used. A third reference results in marginal increase in the estimate uncertainty. The increase in uncertainty can be contrasted with the benefit of having additional degrees of freedom from which

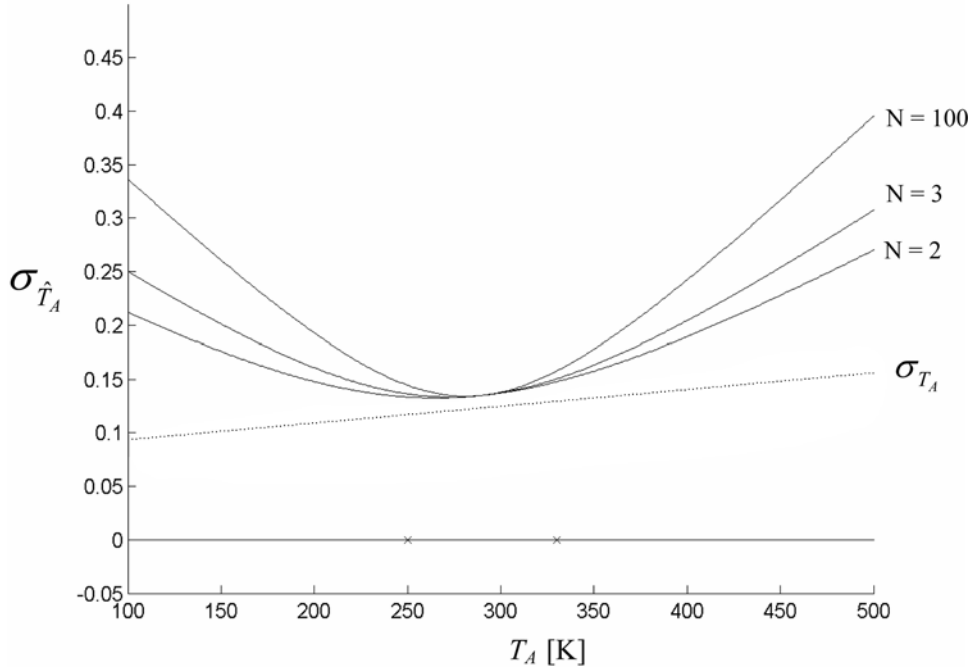


Figure 8. Standard measurement uncertainty as a function of measurand temperature for different numbers of reference temperatures used in the calibration. Reference temperatures are evenly distributed between 250 K and 330 K.

goodness of fit can be obtained by the regression. For example, additional reference measurements may be desired to monitor the linearity of the receiver response. Because the uncertainty will increase for larger latency intervals one should anticipate the uncertainty to be worse if adding additional references results in increased latency. The effect is easy to calculate given a model for the latency interval as a function of N .

6.3. Reference Averaging

[48] In this section the effect of reference averaging on a calibration scheme is examined. Two cases are considered. In the first case a single reference and measurand observations are interleaved. The results are shown to be consistent with previously published results when the measurand and reference are at the same temperature. In the second case, reference averaging is applied to a calibration scheme which switches between three references and the measurand.

[49] A sequence of measurements is shown in Figure 9a, where observations of the measurand and a single reference are interleaved. The measurand and reference temperatures are T_A and T_{ref} , respectively. The cycle period is $\tau = 1$ s, during which time the reference is observed for τ_i s and the measurand is observed for $\tau_A = \tau - \tau_i$. An estimate of the calibration is obtained from n observations of the reference made over an interval $T_W =$

$n\tau$. In order to derive an estimate of the receiver response at least two reference temperatures need to be observed. Hence a second calibration measurement at temperature, T_2 , is assumed to occur outside the interval T_W ; the temperature T_2 is different than T_{ref} . The uncertainty of this second calibration measurement is assumed to be zero, that is, $\sigma_{\hat{T}_2} = 0$, in order to minimize its influence on the calculation of measurement uncertainty. In this example, $B = 20$ MHz and $T_{rec} = 500$ K are assumed. The uncertainties of the measurand and reference observations are calculated using (33). The measurement uncertainty of a single measurand observation is calculated using (29) and then divided by $\sigma = (T_A + T_{rec}) \cdot (B\tau)^{-0.5}$ to obtain the uncertainty relative to the total power mode observation with perfect calibration.

[50] The relative uncertainty for the measurement sequence shown in Figure 9a is plotted in Figure 9b. The results shown are for the balanced case where the reference and measurand are the same, that is, $T_A = T_{rec} = 300$ K. The results do not depend on the temperature of the second calibration reference, T_2 . For $T_W = 1$ and $\tau_i = 0.5$ s the calculations predict the relative uncertainty is equal to that of a Dicke radiometer with a 50% duty cycle, that is, two times that of a total power mode observation of the measurand. The dashed curve in Figure 9b was calculated using equations (16) and (17) from Bremer [1979] which gives the minimum resolution

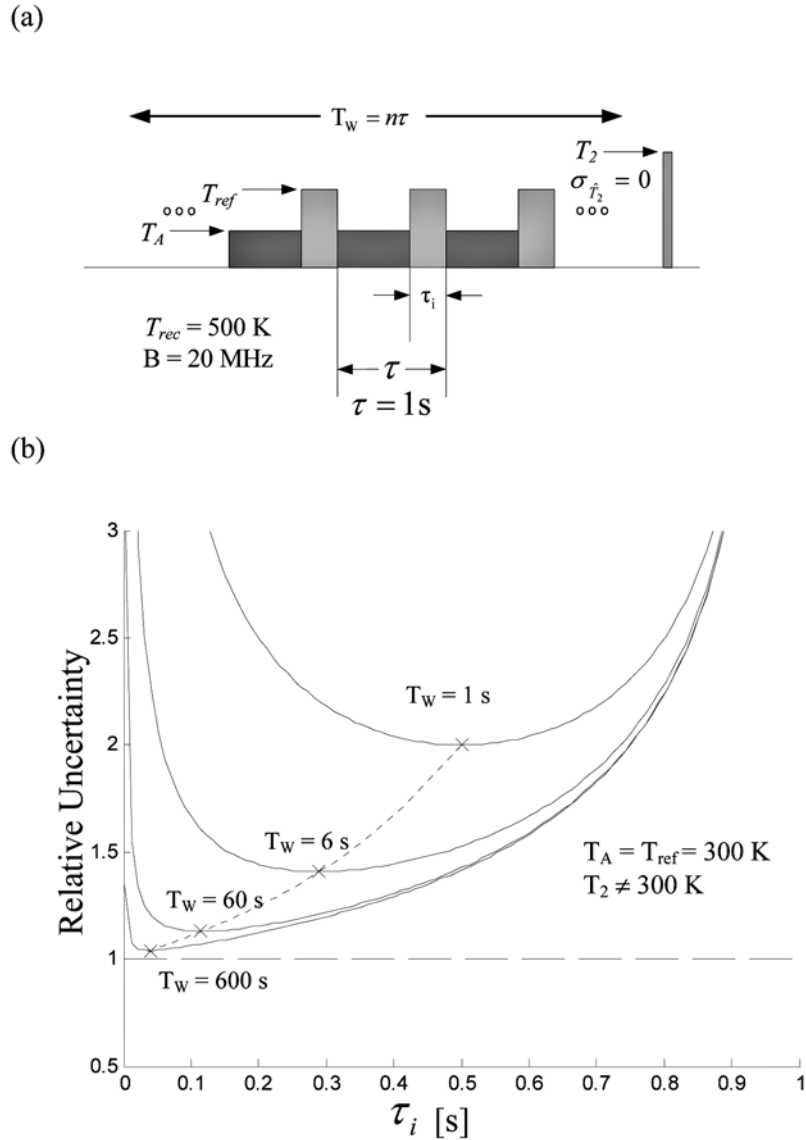


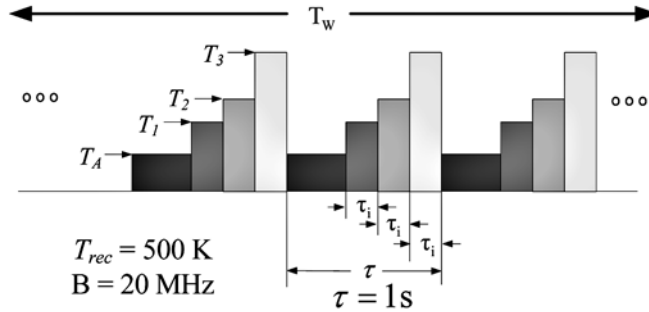
Figure 9. (a) Diagram of a time series of measurements from a single-reference switched radiometer. Reference averaging is applied to the reference measurements over an interval T_w . A second reference, T_2 , is observed with zero uncertainty outside the interval T_w . (b) Relationship between the reference-averaging window width, the reference integration time, and relative uncertainty for the case when $T_{ref} = T_A = 300$ K. The dashed curve indicates the minimum as predicted by *Bremer* [1979].

for a balanced ($T_A = T_{ref}$) switched reference radiometer with asymmetric switching. The results of the LSR analysis for the balanced case are consistent with those of *Bremer*. However, for the unbalanced case, that is, $T_{ref} \neq T_A$, the techniques do not agree; the magnitude and sign of the difference in the techniques depend upon the values used in the calculations. *Bremer's* formula [see

Bremer, 1979, equation (4)] expresses the uncertainty as the root-sum-square of the resolutions of the measurand and reference measurements and does not account for uncertainty in the estimate of the receiver response.

[51] Figure 10a shows a representative sequence of measurements from a switched three-reference radiometer. The three-reference temperatures are $T_1 = 300$ K,

(a)



(b)

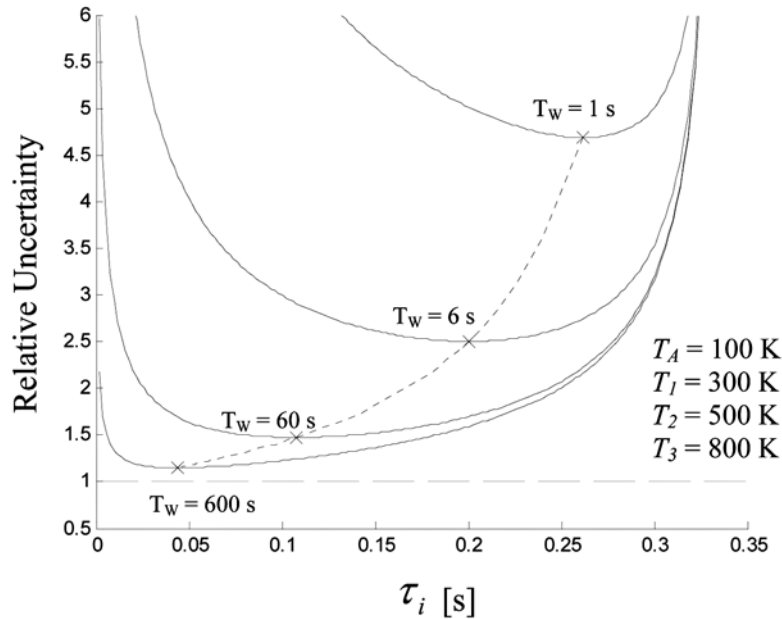


Figure 10. (a) Diagram of a time series of measurements illustrating a window over which reference-averaging is applied to the calibration measurements. (b) Relationship between the reference-averaging window width, the calibration reference integration time, and relative uncertainty. The dashed curve is the minimum relative uncertainty calculated over a range of T_w .

$T_2 = 500$ K and $T_3 = 800$ K. The receiver noise temperature is $T_{rec} = 500$ K and the predetection bandwidth is 20 MHz. The time spent calibrating, $3\tau_i$, is split evenly between the three references; the cycle period is $\tau = 1$ s and the measurand is observed for $\tau_A = \tau - 3\tau_i$; latency due to switching between references is assumed negligible. The measurand brightness temperature is $T_A = 100$ K. The relative uncertainty is calculated the same way as in Figure 9b.

[52] Figure 10b illustrates the relationship between the calibration integration time and measurement uncertainty for different observation window lengths, T_w , over which reference measurements are used for calibration. The measurement uncertainty has been normalized by the radiometric resolution of a total power measurement with a 1 s integration time. The curve for $T_w = 1$ s corresponds to a single set of calibration measurements, $n = N = 3$, and yields a minimum uncertainty of ~ 4.7 times that

of the resolution in total power mode. In this case the measurand is viewed only $\sim 21\%$ of the cycle period. The dashed line indicates the minimum uncertainty as a function of calibration integration time and observation window. Dramatic improvement in measurement uncertainty results by increasing the window over which multiple calibration measurements can be used. Improvement in measurement uncertainty results partly from the increased fraction of time spent observing the measurand and to a greater extent from improving the estimate of the system response. For a 10 min window, $T_W = 600$ s, the minimum relative uncertainty is 1.16. When considering large observation windows one should be concerned with the nonstationary fluctuations in the receiver. Calculations using a nonstationary model for the receiver fluctuations (not shown in this paper) reveal that the shapes of the curves in Figure 10b are largely unaffected; however, for long averaging intervals the curves are shifted upward yielding greater measurement uncertainty.

7. Discussion

[53] In the preceding sections, a technique is described that uses measurement uncertainty as a figure of merit to assess the performance of a variety of radiometer designs. The technique can be applied to radiometer designs that can be decomposed into a set of total power mode receiver subsystems; the output of each subsystem is a random process described by a characteristic equation. The radiometer output is a sequence of samples from the different random processes. An estimator for the measurand is derived from samples of the different subsystems. Measurement uncertainty is calculated from the functional form of the estimator and the statistics of the random variables comprising the estimator.

[54] The form that the estimator can take depends on the radiometer design and its sampled states. In this paper least squares regression is used as a convenient framework to demonstrate the utility of measurement uncertainty as a figure of merit. The LSR approach offers a number of advantages. LSR minimizes the measurement error in the least squares sense and can be applied to a wide variety of calibration designs for performing trade-off studies of design parameters. LSR provides a simple and straightforward way of computing the measurement uncertainty in terms of parameters (e.g., standard uncertainty of the calibration measurements) convenient for interpretation; the linear algebra required to compute the measurement uncertainty is easily programmed. The influence of applying weights to the calibration measurements can be evaluated using weighted LSR. For calibration measurements characterized by Gaussian statistics, the optimum weights are inversely proportional to the standard uncertainty of the calibration measurements.

When the calibration measurements are correlated, generalized LSR can be used to include the influence of their correlation.

[55] Methods other than LSR are often used to form an estimator and many calibration implementations are not readily expressed as a set of equations in the form of (21) that can be solved by LSR. For example, consider a radiometer that alternately couples noise into the antenna measurement path and a set of external calibration measurements (tier 3) are used to estimate the value of additive noise. The functional form of the estimator would not include the coupled noise value but rather be a function of the external calibration measurements. The uncertainty in the estimator would then include uncertainty associated with the external calibration measurements. It should be noted that the functional form of the estimator in (28) does not include the slope and offset but does include those random variables (i.e., calibration measurements) from which the slope and offset are estimated. Regardless of the system architecture, an estimator of the measurand will take a functional form; the functional form can then be used to calculate the measurement uncertainty based on the stochastic properties of the variables that comprise the estimator.

[56] When modeling the measurement uncertainty for a design study, one has freedom in assigning the value of uncertainty to each component that contributes uncertainty. Consider for example a design analysis in which a noise source exhibits thermal instability; the uncertainty associated with the noise source measurement can be adjusted and its influence on the measurement uncertainty understood. One can then choose to modify the calibration design or functional form of the estimator to compensate for anticipated noise source instability. Thereby, analysis of measurement uncertainty based on stochastic models of anticipated fluctuations can be a valuable aid in understanding the influence of component characteristics on system performance.

[57] Periodic calibration is required to correct for nonstationary fluctuations in the receiver response, for example, drifts in receiver gain. In this presentation temporal effects such as time interval between calibrations are not considered. This omission is not a limitation of the approach presented. Generally, the uncertainty in the calibration measurement will increase as the interval between the time a calibration measurement is made and the time onto which it is applied increases. The amount by which the uncertainty grows is a function of the nonstationary stochastic properties of the receiver response. The influence of nonstationary fluctuations in the receiver can be assessed by treating the set (or subset) of random processes from which the radiometer output is sampled as nonstationary. The technique outlined in this paper provides a powerful means for studying the nature of nonstationarity in radiometer systems.

[58] In this paper measurement uncertainty is introduced as a figure of merit to evaluate radiometer designs. As with most figures of merit, one must use discretion in their application for judging performance; other factors may also be important. For some measurements, resolution of the measurand observation may be more important than the measurement accuracy; alternatively, maintaining the ability to monitor system linearity by means of a multipoint calibration may take precedence. Regardless, measurement uncertainty is a quantitative measure that can be used for assessing radiometer designs.

8. Conclusion

[59] Previously radiometric resolution has been used as a figure of merit to assess the performance of radiometer designs. Radiometric resolution is an important parameter to consider when designing a radiometer; however, difficulties arise when using resolution to evaluate the performance of a calibration design. The evaluation of the ensemble averages required to find the variance of the output signal is complicated by the switching of the input signal between multiple sources. Radiometric resolution is defined and evaluated for a single system temperature (T_{sys}) and mean system response. Thus the theoretical basis for using radiometric resolution to characterize the performance of a calibration design is questionable since calibration inevitably involves changing the system temperature to derive estimates of the system response; uncertainty in the estimate of the system response is unavoidable. Measurement uncertainty is a more appropriate figure of merit for assessing the performance of a radiometer and its calibration. Measurement uncertainty includes the radiometric resolution of the measurand observation as well as the uncertainty associated with utilizing imperfect calibration data.

[60] A general radiometer calibration model is introduced that describes a wide variety of calibration architectures. Most radiometers contain calibration features from one or more of the three tiers identified by the model. Regardless from which tier an observation is made, the observed signal can be modeled by a random process; all signals observed are treated as originating from simultaneously existing random processes. The radiometer output thus comprises a sequence of samples obtained from a set of different random processes. The statistics of the calibration reference and measurand samples are derived from the properties of the underlying random processes. The statistics are then used with the functional form of the calibration algorithm to compute the measurement uncertainty. The technique presented can be applied to all radiometer designs that can be decomposed into a set of subsystems that represent total power mode observations.

[61] LSR is used as a framework for modeling the calibration algorithm although the theoretical basis for using measurement uncertainty to assess the performance of radiometer designs extends to a broader class of calibration algorithms. The utility of measurement uncertainty as a figure of merit is demonstrated by evaluating the influence of calibration reference temperatures, number of calibration references, integration time of the calibration references, integration time of the measurand, and reference averaging. The technique presented has been applied to evaluating calibration designs using two and more calibration references and to systems utilizing reference averaging. The effect of interpolating and extrapolating calibration data on measurement uncertainty is shown. The optimum fraction of time spent observing the measurand is shown to depend on the calibration reference temperatures.

[62] This work focused on developing techniques for radiometer design analysis based on stochastic models of anticipated fluctuations within the radiometer and hence is limited to type B uncertainty analysis. For analyzing the measurement uncertainty of actual radiometer systems, the statistical analysis of series of observations should be considered.

Appendix A: Derivation of Resolution for a Radiometer Receiver With Gain Fluctuations

[63] In this appendix the radiometric resolution is evaluated for a direct detection radiometer with gain fluctuations operating in total power mode. A model for such a radiometer is shown in Figure 2 and described in section 3. The input signal to the radiometer receiver, $x(t)$, is assumed to be a zero mean Gaussian random process with a white noise power spectrum given by

$$S_x(f) = kT_{sys}, \quad (A1)$$

where k is Boltzman's constant and T_{sys} is the system noise temperature. The system noise temperature is equal to the sum of the receiver noise temperature (T_{rec}) and the apparent antenna temperature (T_p) at the radiometer input, that is, $T_{sys} = T_{rec} + T_p$. The impulse responses of the predetection and postdetection filters are $h(t)$ and $w(t)$, respectively. The frequency responses of the filters are given by the Fourier transform pairs

$$W(f) = \int_{-\infty}^{\infty} w(t)e^{-i\omega t} dt, \quad H(f) = \int_{-\infty}^{\infty} h(t)e^{-i\omega t} dt, \quad (A2)$$

where $\omega = 2\pi f$. The bandwidth of the predetection filter is assumed to be much larger than the bandwidth of the

postdetection filter. The amplifier gain is expressed as the sum of the mean and a fluctuating component, that is,

$$g(t) = g_0 + \tilde{g}(t), \quad (\text{A3})$$

where g_0 is the mean value of $g(t)$ and $\tilde{g}(t)$ is the fluctuating component. The fluctuating component is modeled as a zero mean Gaussian random process. By assuming $\tilde{g}(t)$ is wide sense stationary, the Fourier transform relationship between its autocorrelation function and power spectrum exists, such that

$$E\{\tilde{g}(t_1)\tilde{g}^*(t_2)\} \equiv R_{\tilde{g}}(\Delta t) = \int_{-\infty}^{\infty} S_{\tilde{g}}(f)e^{j\omega\Delta t}df, \quad (\text{A4})$$

where $\Delta t = t_2 - t_1$, $*$ denotes the complex conjugate, and $R_{\tilde{g}}(\Delta t)$ and $S_{\tilde{g}}(f)$ are the autocorrelation and power spectrum of $\tilde{g}(t)$, respectively. In the following analysis, it is assumed that $g(t)$ and $x(t)$ are independent and that the fluctuation in $\tilde{g}(t)$ is much slower than the impulse response of $h(t)$. The fluctuation can exist on the same timescale as the impulse response of the postdetection filter.

[64] The receiver input passes through an amplifier, filter, and an ideal square law detector. The output of the square law detector is denoted $y(t)$, and $v(t)$ is the voltage output of the postdetection filter. By assuming the gain fluctuations are slow, the output of the amplifier can be expressed as the instantaneous product $x(t)g(t)$. The output of the square law detector is

$$y(t) = c(x(t)g(t) \otimes h(t))^2, \quad (\text{A5})$$

where \otimes is the convolution operator, c is the gain of the square law detector (usually expressed in units of volts per watts). The output of the postdetection filter is

$$\begin{aligned} v(t) &= y(t) \otimes w(t) \\ &= c \cdot \int_{-\infty}^{\infty} dt''' w(t''') \int_{-\infty}^{\infty} dt' h(t') \\ &\quad \cdot \int_{-\infty}^{\infty} dt'' h(t'') x(t - t' - t''') \\ &\quad \cdot g(t - t' - t''') x(t - t'' - t''') g(t - t'' - t'''). \end{aligned} \quad (\text{A6})$$

By making use of the Fourier relationships and the above stated assumptions (i.e., $x(t)$ is zero mean Gaussian and $\tilde{g}(t)$ and $w(t)$ are slow with respect to $h(t)$) the expected value of the output is found to be

$$\begin{aligned} E\{v(t)\} &= \bar{v}_p \\ &= ckW(0)T_{\text{sys}} \cdot \left(\int df |H(f)|^2 \right) \cdot (g_0^2 + R_{\tilde{g}}(0)). \end{aligned} \quad (\text{A7})$$

The ensemble average includes all possible output voltages that correspond to system noise temperature. Equation (A7) shows the linear relationship between the input brightness temperature to the output voltage. This linear relationship arises from the square law detection of the input signal. Equation (A7) can be rewritten to explicitly show the linear relationship,

$$\bar{v}_p = \mu T_p + \beta, \quad (\text{A8})$$

where

$$\mu = ckW(0) \left(\int df |H(f)|^2 \right) \cdot (g_0^2 + R_{\tilde{g}}(0)) \quad (\text{A9})$$

and

$$\beta = \mu T_{\text{rec}}. \quad (\text{A10})$$

[65] The resolution is found by evaluating (6). First consider the denominator; differentiating (A7) with respect to T_{sys} one finds

$$\left(\frac{\partial}{\partial T} E\{v(t)\} \right) \Big|_{T=T_{\text{sys}}} = \mu^2, \quad (\text{A11})$$

where μ is given by (A9).

[66] Evaluation of the numerator is more involved since it requires finding the variance of the output, which in turn involves evaluating the fourth-moment statistics of $g(t)$ and $x(t)$. The variance is found from the zero lag covariance function of the receiver output. The covariance function is given by

$$\begin{aligned} E\{v(t_1)v^*(t_2)\} &= C_v(\Delta t) \\ &= \int_{-\infty}^{\infty} S_y(f) |W(f)|^2 e^{-j\omega\Delta t} df \\ &\quad - E^2\{v(t)\} \Big|_{T=T_{\text{sys}}}, \end{aligned} \quad (\text{A12})$$

where $S_y(f)$ is the power spectrum at the output of the square law detector and is found from the Fourier transform of the autocorrelation function

$$R_y(\Delta t) = E\{y(t_1)y^*(t_2)\}. \quad (\text{A13})$$

Evaluating (A13) requires calculating the fourth-moment expected averages of $x(t)$ and $g(t)$. In this calculation the relationship

$$E\{x(t_1)x(t_2)x(t_3)x(t_4)\} = R_{x_{12}}R_{x_{34}} + R_{x_{13}}R_{x_{24}} + R_{x_{14}}R_{x_{23}} \quad (\text{A14})$$

for zero mean Gaussian random processes is used where $R_{x_{ij}} = E\{x(t_i)x(t_j)\}$. To evaluate (A13), substitute the

corresponding Fourier transforms for $R_x(\bullet)$ and $R_{\bar{g}}(\bullet)$, apply the Fourier exponents to transform the filter impulse responses to the frequency domain, utilize the assumption that the bandwidth of $H(f)$ is much larger than the bandwidth of $S_{\bar{g}}(f)$, and term by term use the remaining integrals to transform the power spectrum of the gain fluctuations back into the time domain. After grouping like terms,

$$R_y(\Delta t) = c^2 R_H^2(0) \cdot \left[g_0^4 + 2g_0^2 R_{\bar{g}}(0) + R_{\bar{g}}^2(0) + 2R_{\bar{g}}^2(\Delta t) + 4g_0^2 R_{\bar{g}}(\Delta t) \right] + 2c^2 R_H^2(\Delta t) \cdot \left[g_0^4 + 2g_0^2 R_{\bar{g}}(0) + R_{\bar{g}}^2(0) + 2R_{\bar{g}}^2(\Delta t) + 4g_0^2 R_{\bar{g}}(\Delta t) \right], \quad (\text{A15})$$

where

$$R_H(\Delta t) = \int_{-\infty}^{\infty} S_x(f) |H(f)|^2 e^{j\omega\Delta t} df.$$

[67] By subtracting the DC component from (A15), (A12) may be expressed as

$$C_v(\Delta t) = \int_{-\infty}^{\infty} S_r(f) |W(f)|^2 e^{j\omega\Delta t} df, \quad (\text{A16})$$

where

$$S_r(f) = 2c^2 R_H^2(0) (S_{\bar{g}} \otimes S_{\bar{g}}) + 4c^2 R_H^2(0) g_0^2 S_{\bar{g}} + \left(2c^2 g_0^4 + 6c^2 R_{\bar{g}}^2(0) + 12c^2 g_0^2 R_{\bar{g}}(0) \right) \cdot S_H \otimes S_H$$

and S_H is the Fourier transform of R_H . The variance of the output is found by evaluating (A16) with $\Delta t = 0$. It is noteworthy to observe that the variance obtained from (A16) is the starting point for analysis presented by *Hersman and Poe* [2000].

[68] Substituting (A1) into (A16) and making use of the bandwidth assumption between the predetection and postdetection filters yields

$$C_v(\Delta t) = \left[\left(g_0^4 + 3R_{\bar{g}}^2(0) + 6g_0^2 R_{\bar{g}}(0) \right) 2c^2 k^2 T_{\text{sys}}^2 \int_{-\infty}^{\infty} df' |H(f')|^4 \int_{-\infty}^{\infty} df |W(f)|^2 e^{j\omega\Delta t} + 4c^2 g_0^2 k^2 T_{\text{sys}}^2 \left[\int_{-\infty}^{\infty} df' |H(f')|^2 \right]^2 \int_{-\infty}^{\infty} df''' |W(f''')|^2 S_{\bar{g}}(f''') e^{j\omega\Delta t} \right] \cdot W^2(0) R_{\bar{g}}(\Delta t). \quad (\text{A17})$$

The first term on the right-hand side of (A17) is the covariance due to the band-limited noise at the receiver input; this term gives rise to (7) and its correlation interval is governed by the bandwidth of the postdetection filter. Receiver gain fluctuations give rise to the second term on the right-hand side. For gain fluctuations that are slow with respect to Δt and small in magnitude compared to g_0 , the covariance function of the receiver output can be expressed as

$$C_v(\Delta t) = 2g_0^4 c^2 k^2 T_{\text{sys}}^2 \int_{-\infty}^{\infty} df' |H(f')|^4 R_W(\Delta t) + 4c^2 g_0^2 k^2 T_{\text{sys}}^2 \left[\int_{-\infty}^{\infty} df' |H(f')|^2 \right]^2 \cdot W^2(0) R_{\bar{g}}(\Delta t), \quad (\text{A18})$$

where

$$R_W(\Delta t) = \int_{-\infty}^{\infty} df |W(f)|^2 e^{j\omega\Delta t}. \quad (\text{A19})$$

[69] The covariance function given by (A18) is a linear combination of R_W and $R_{\bar{g}}$ scaled by g_0^4 and g_0^2 , respectively. The contribution of $R_{\bar{g}}$ is usually negligible for computing the output variance since receiver gain fluctuations are typically small over the integration interval defined by $W(f)$. The contribution of R_W to the covariance between sequential samples, for example, calibration observations, is usually very small since R_W tends to decay rapidly on timescales longer than the sampling interval. Gain fluctuations become more predominant for the covariance between samples as the time interval increases. Although we have assumed stationarity, one must keep in mind that gain fluctuations are inherently nonstationary; $R_{\bar{g}}(\Delta t)$ may not adequately represent the gain fluctuations since it is an autocorrelation function of a wide sense stationary process. The covariance function given by (A17) is valid for time intervals over which the fluctuations can be considered stationary. It should be noted that the covariance given by (A17) changes slightly when the time interval encompasses observations at two different system temperatures, that is, $T_{\text{sys}}^2 \rightarrow T1 \cdot T2$ where $T1$ and $T2$ are the system temperatures at the two times.

[70] The radiometric resolution is obtained by substituting (A11) and the variance obtained from (A17) into (6). The following definitions are adopted from *Tiuri* [1964]. The predetection bandwidth is

$$B = \frac{\left(\int_{-\infty}^{\infty} |H(f)|^2 df \right)^2}{\int_{-\infty}^{\infty} |H(f)|^4 df}, \quad (\text{A20})$$

and the postdetection integration time constant is

$$\tau = \frac{W^2(0)}{2 \int_{-\infty}^{\infty} |W(f)|^2 df}. \quad (\text{A21})$$

After making the substitutions

$$\left(\frac{\Delta T}{T_{\text{sys}}}\right)^2 = \frac{2 \int_{-\infty}^{\infty} (S_{\bar{g}} \otimes S_{\bar{g}} + 2g_0^2 S_{\bar{g}}) |W(f)|^2 df}{(g_0^2 + R_{\bar{g}}(0))^2 W^2(0)} + \left(\frac{g_0^4 + 3R_{\bar{g}}^2(0) + 6g_0^2 R_{\bar{g}}(0)}{(g_0^2 + R_{\bar{g}}(0))^2}\right) \frac{1}{B\tau}. \quad (\text{A22})$$

By making the assumption that the mean gain is much larger than the gain fluctuations, that is, $g_0^2 \gg R_{\bar{g}}(0)$, (A22) can be further simplified to obtain (8).

[71] It is interesting to see how (A22) relates to other published forms of resolution for receivers with gain fluctuations [Ulaby et al., 1981; Rohlfis and Wilson, 1996]. To do this, assume that the voltage gain is a Gaussian random variable and substitute $S_{\bar{g}}(f) = \sigma_{\bar{g}}^2 \delta(f)$ into (A22), where $\delta(f)$ is the Dirac delta function. Next define the power gain as $G = g^2$. Using the properties of the Gaussian random variable [Davenport and Root, 1987], the power gain is also a random variable with mean

$$G_0 = E\{G\} = E\{g^2\} = g_0^2 + \sigma_{\bar{g}}^2 \quad (\text{A23})$$

and variance

$$(\Delta G)^2 = E\{(G - G_0)^2\} = 2\sigma_{\bar{g}}^4 + 4g_0^2 \sigma_{\bar{g}}^2. \quad (\text{A24})$$

Upon substituting these definitions into (A22), one obtains

$$\left(\frac{\Delta T}{T_{\text{sys}}}\right)^2 = \left(\frac{\Delta G}{G_0}\right)^2 + \frac{1}{B\tau}. \quad (\text{A25})$$

[72] **Acknowledgments.** The authors would like to thank Ed Westwater for valuable discussions that contributed to the development of the work presented. The authors would also like to thank David Le Vine, Jeffrey Piepmeier, and the *Radio Science* reviewers for their insightful comments that led to improvements in the paper. This work was conducted in support of NASA's Earth Science Enterprise at the Goddard Space Flight Center.

References

American National Standards Institute (ANSI) (1997), American national standard for calibration—U.S. guide to the expression of uncertainty in measurement, *ANSI/NCSL Z540-2-1997*, Natl. Conf. of Stand. Lab., Boulder, Colo.

- Blackwell, W. J., J. W. Barrett, F. W. Chen, R. V. Leslie, P. W. Rosenkranz, M. J. Schwartz, and D. H. Staelin (2001), NPOESS Aircraft Sounder Testbed-Microwave (NASt-M): Instrument description and initial flight results, *IEEE Trans. Geosci. Remote Sens.*, 39(11), 2444–2453.
- Bremer, J. (1979), Improvement of scanning radiometer performance by digital reference averaging, *IEEE Trans. Instrum. Meas.*, 28(1), 46–54.
- Buderi, R. (1996), *The Invention That Changed the World: How a Small Group of Radar Pioneers Won the Second World War and Launched a Technological Revolution*, Simon and Schuster, New York.
- Conglong, Z., J. B. Snider, and D. C. Hogg (1986), Computer demodulation technique for a dual-channel microwave radiometer, *Adv. Atmos. Sci.*, 3(2), 189–198.
- Corbella, I., A. J. Gasiewski, M. Klein, V. Leuski, A. J. Francavilla, and J. R. Piepmeier (2002), On-board accurate calibration of dual-channel radiometers using internal and external references, *IEEE Trans. Microwave Theory Tech.*, 50(7), 1816–1820.
- Davenport, W. B., and W. Root (1987), *An Introduction to the Theory of Random Signals and Noise*, IEEE Press, Piscataway, N. J.
- Davis, A., A. Marshak, W. Wiscombe, and R. Cahalan (1996), Scale invariance of liquid water distribution in marine stratocumulus, part 1: Spectral properties and stationary issues, *J. Atmos. Sci.*, 53(11), 1538–1558.
- Dicke, R. H. (1946), The measurement of thermal radiation at microwave frequencies, *Rev. Sci. Instrum.*, 17, 268–279.
- Draper, N. R., and H. Smith (1998), *Applied Regression Analysis*, 3rd ed., John Wiley, Hoboken, N. J.
- Hach, J. P. (1968), A very sensitive airborne microwave radiometer using two reference temperatures, *IEEE Trans. Microwave Theory Tech.*, 16(9), 629–636.
- Han, Y., and E. R. Westwater (2000), Analysis and improvement of tipping calibration for ground-based microwave radiometers, *IEEE Trans. Geosci. Remote Sens.*, 38(3), 1260–1276.
- Hersman, M. S., and G. A. Poe (2000), Sensitivity of the total power radiometer with periodic absolute calibration, *IEEE Trans. Microwave Theory Tech.*, 29(1), 32–40.
- Huang, N. E., Z. Shen, S. R. Long, M. C. Wu, H. S. Hsing, Q. Zheng, N.-C. Yen, C. C. Tung, and H. H. Liu (1998), The empirical mode decomposition and the Hilbert spectrum for nonlinear and non-stationary time series analysis, *Proc. R. Soc. London, Ser. A*, 454, 903–995.
- Institute of Electrical and Electronics Engineers (1996), The IEEE standard dictionary of electrical and electronic terms, *IEEE Stand. 100*, Piscataway, N. J.
- International Organization for Standardization (ISO) (1993), *International Vocabulary of Basic and General Terms in Metrology*, 2nd ed., Int. Org. for Stand., Geneva, Switzerland.
- Kelly, E. J., D. H. Lyons, and W. L. Root (1963), The sensitivity of radiometric measurements, *J. Soc. Ind. Appl. Math.*, 11(2), 235–257.

- Kraus, J. D. (1966), *Radio Astronomy*, Cygnus Quasar, Powell, Ohio.
- Kunzi, K., and A. Magun (1977), Statistical gain fluctuations of microwave amplifiers measured with a Dicke-radiometer, *Math. Phys.*, 22, 404–411.
- Le Vine, D. M. (1990), The sensitivity of synthetic aperture radiometers for remote sensing applications from space, *Radio Sci.*, 25(4), 441–453.
- Liljegren, J. C. (2000), Automatic self-calibration of ARM microwave radiometers, in *Microwave Radiometry and Remote Sensing of the Earth's Surface and Atmosphere*, edited by P. Pampaloni and S. Paloscia, pp. 433–441, VSP, Leiden, Netherlands.
- McGrath, A., and T. Hewison (2001), Measuring the accuracy of MARSS—An airborne microwave radiometer, *J. Atmos. Oceanic Technol.*, 18(12), 2003–2012.
- Miller, C. K. S., W. C. Daywitt, and M. G. Arthur (1967), Noise standards, measurements, and receiver noise definitions, *Proc. IEEE*, 55(6), 865–877.
- Peckham, G. E. (1989), An optimum calibration procedure for radiometers, *Int. J. Remote Sens.*, 10(1), 227–236.
- Racette, P., and J. R. Wang (1998), Passive millimeter- and sub-millimeter-wave imaging for atmospheric research, paper presented at International Society for Optical Engineering 12th Annual Symposium, Orlando, Fla., April.
- Racette, P., J. R. Wang, P. Evans, R. Saunders, A. Gasiewski, and D. Jackson (1995), A calibration experiment using millimeter-wave imaging radiometer at the UK meteorological office calibration facility, paper presented at International Geophysics and Remote Sensing Symposium '95, Inst. of Electr. and Electron. Eng., Florence, Italy, July.
- Racette, P., R. F. Adler, J. R. Wang, A. J. Gasiweski, D. M. Jackson, and D. S. Zacharias (1996), An airborne millimeter-wave imaging radiometer for cloud, precipitation, and atmospheric water vapor studies, *J. Atmos. Oceanic Technol.*, 13(3), 610–619.
- Racette, P., M. Triesky, and D. C. Jones (1998), A multi-channel microwave radiometer uses reference averaging for calibration: Precision approaches that of a total power radiometer, paper presented at International Geophysics and Remote Sensing Symposium '98, Inst. of Electr. and Electron. Eng., Seattle, Wash., July.
- Randa, J. (1998), Uncertainties in NIST noise measurements, *Tech. Note 1502*, Natl. Inst. of Stand. and Technol., Gaithersburg, Md.
- Rohlfs, K., and T. L. Wilson (1996), *Tools of Radio Astronomy*, Springer, New York.
- Ruf, C. S. (2000), Detection of calibration drifts in spaceborne microwave radiometers using a vicarious cold reference, *IEEE Trans. Geosci. Remote Sens.*, 38(1), 44–52.
- Ruf, C. S., S. J. Keihm, and M. A. Janssen (1995), TOPEX/Poseidon Microwave Radiometer (TMR): I. Instrument description and antenna temperature calibration, *IEEE Trans. Geosci. Remote Sens.*, 33(1), 125–137.
- Saunders, R. W., T. J. Hewison, S. J. Stringer, and N. C. Atkinson (1995), The radiometric characterization of AMSU-B, *IEEE Trans. Microwave Theory Tech.*, 43(4), 760–771.
- Skou, N. (1989), *Microwave Radiometer Systems: Design and Analysis*, Artech House, Norwood, Mass.
- Stelzried, C. T. (1968), Microwave thermal noise standards, *IEEE Trans. Microwave Theory Tech.*, 16(9), 646–655.
- Tanner, A. B., and A. L. Riley (2003), Design and performance of a high-stability water vapor radiometer, *Radio Sci.*, 38(3), 8050, doi:10.1029/2002RS002673.
- Thomsen, F. (1984), On the resolution of Dicke-type radiometers, *IEEE Trans. Microwave Theory Tech.*, 32(2), 145–150.
- Tiuri, M. E. (1964), Radio astronomy receivers, *IEEE Trans. Mil. Electron.*, 8, 264–272.
- Ulaby, F. T., R. K. Moore, and A. K. Fung (1981), *Microwave Remote Sensing: Active and Passive*, vol. 1, *Microwave Remote Sensing Fundamentals and Radiometry*, Addison-Wesley, Boston, Mass.
- Van Putten, A. F. P. (1996), *Electronic Measurement Systems, Theory and Practice*, pp. 110–152, Inst. of Phys., Philadelphia, Pa.
- Wait, D. F. (1967), The sensitivity of the Dicke radiometer, *J. Res. Natl. Bur. Stand.*, 71(2), 127–152.
- Wentz, F. J., P. Ashcroft, and C. Gentemann (2001), Post-launch calibration of the TRMM microwave imager, *IEEE Trans. Geosci. Remote Sens.*, 39(2), 415–422.

R. H. Lang, Dept. of Electrical Engineering and Computer Science, George Washington University, Phillips Hall, Washington, DC 20052, USA. (lang@gwu.edu)

P. Racette, NASA Goddard Space Flight Center, Code 555, Greenbelt, MD 20771, USA. (paul.e.racette@nasa.gov)